THE JOURNAL OF PHYSICAL CHEMISTRY C

Article

pubs.acs.org/JPCC

Volatilities of Actinide and Lanthanide *N,N*-Dimethylaminodiboranate Chemical Vapor Deposition Precursors: A DFT Study

Bess Vlaisavljevich,[†] Pere Miró,[†] Drew Koballa,[†] Tanya K. Todorova,[‡] Scott R. Daly,[§] Gregory S. Girolami,*[,§] Christopher J. Cramer,[†] and Laura Gagliardi*[,†]

[†]Department of Chemistry, Supercomputing Institute, and Chemical Theory Center, University of Minnesota, 207 Pleasant Street SE, Minneapolis, Minnesota 55455, United States

[‡]Ecole Polytechnique Federale de Lausanne (EPFL), Institute of Chemical Sciences and Engineering, Laboratory for Computational Molecular Design, 1015 Lausanne, Switzerland

[§]The School of Chemical Sciences, University of Illinois at Urbana−Champaign, 600 South Mathews Avenue, Urbana, Illinois 61801, United States

Supporting Information

ABSTRACT: *N,N*-Dimethylaminodiboranate complexes with praseodymium, samarium, erbium, and uranium, which are potential chemical vapor deposition precursors for the deposition of metal boride and oxide thin films, have been investigated by DFT guided by field-ionization mass spectroscopy experiments. The calculations indicate that the volatilities of these complexes are correlated with the M−H bond strengths as determined by Mayer bond order analysis. The geometries of the gas-phase monomeric, dimeric, and trimeric species seen in field-ionization mass spectroscopy experiments were identified using DFT calculations, and the relative stabilities of these oligomers were assessed to understand how the lanthanide aminodiboranates depolymerize to their respective volatile forms during sublimation.

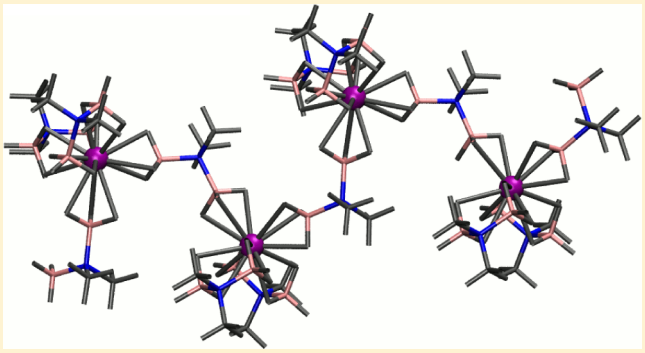

INTRODUCTION

Lanthanide-containing materials, such as lanthanide oxides and borides, have interesting optical,[1−3] magnetic,[4−6] and electrical[4,7,8] properties that make them useful for technological applications such as capacitors, field effect transistors, displays, thermoelectric devices, light-emitting diodes, and lasers. For many of these applications, defect-free thin films are necessary, and in some cases it is crucial to deposit the films uniformly onto substrates with high aspect ratios.[9] To achieve these results, there is much interest in developing better precursors for the chemical vapor deposition (CVD) and atomic layer deposition (ALD) of lanthanide-containing thin films.[10,11]

For transition metals, some of the most volatile compounds known are homoleptic compounds containing the borohydride ligand, BH_4^-, and these have been shown to be useful CVD precursors.[12−20] Homoleptic borohydride compounds of the lanthanides are known but they are not particularly volatile[21−25] because their solid state structures are polymeric.[26−28] By comparison, actinide borohydrides in the +4 oxidation state such as $U(BH_4)_4$ are reasonably volatile despite the fact that some of them are also polymeric in the solid state.[29]

Recently, a new class of metal borohydrides has been described that contain the *N,N*-dimethylaminodiboranate anion, $H_3BNMe_2BH_3^-$ (DMADB) (Figure 1).[30−32] DMADB is a polydentate ligand capable of chelating a single metal center or bridging between two metal centers.

Compared to the smaller BH_4^- ligand, the DMADB ligand better saturates the coordination sphere of large metals in lower oxidation states.[31] Consequently, lanthanide complexes containing DMADB ligands are among the most volatile compounds known for these elements.[32,33]

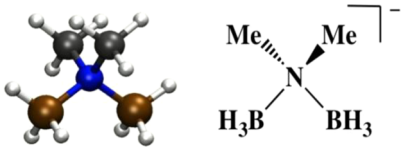

Figure 1. Ball and stick (left) and schematic (right) structure of the *N,N*-dimethylaminodiboranate (DMADB) ligand. Color code: Nitrogen in blue, carbon in gray, boron in bronze, and hydrogen in white.

Received: June 11, 2012
Revised: August 24, 2012
Published: October 5, 2012

dx.doi.org/10.1021/jp305691y | *J. Phys. Chem. C* 2012, 116, 23194−23200

Several $M(DMADB)_3$ complexes with trivalent lanthanides (all except promethium) and an actinide (uranium) have been reported.[31−33] Because the DMADB ligand can chelate to or bridge between two metal centers, a variety of solid-state structures have been observed depending on the size of the M^{3+} ion: the coordination number increases from 12 to 14 as the ionic radius of the metal center becomes larger.[34] As shown in Figure 2, the relatively small erbium ion Er^{3+} (r_{Er} = 0.89 Å) forms a dinuclear structure, $Er_2(DMADB)_6$, in which the Er centers are linked by two bridging DMADB ligands, each end of which forms two Er−H bonds. Additionally, each Er center has two chelating DMADB ligands, each providing four Er−H bonds, giving a total coordination number of 12.

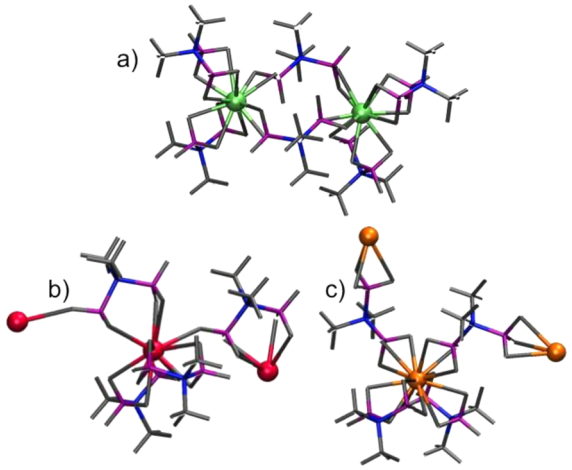

Figure 2. Single crystal X-ray diffraction structures.[31−33] (a) $Er_2(DMADB)_6$ dimer, (b) fragment of the $Sm(DMADB)_3$ or U_A polymeric chain, (c) fragment of the $Pr(DMADB)_3$ or U_B polymeric chain. Color code: Erbium in green, samarium/uranium in red, praseodymium/uranium in orange, nitrogen in blue, boron in magenta, carbon and hydrogen in gray.

For the somewhat larger samarium ion Sm^{3+} (r_{Sm} = 0.96 Å), all three ligands chelate via four Sm−H bonds, but an intermolecular Sm−H bond links the Sm centers together into a chain bringing the total coordination number to 13. In contrast, the even larger praseodymium ion Pr^{3+} (r_{Pr} = 0.99 Å) is coordinated by two chelating DMADB ligands, each of which forms four Pr−H bonds. Moreover, each Pr atom coordinates to two additional bridging DMADB ligands that link the metal centers into a polymeric chain. Each end of the bridging ligands forms three Pr−H bonds resulting in a total coordination number of 14. Finally, for $U(DMADB)_3$, two structural isomers have been synthesized. Isomer U_A is isostructural with 13-coordinate $Sm(DMADB)_3$ and crystallizes from pentane, whereas isomer U_B is isostructural with 14-coordinate $Pr(DMADB)_3$ and crystallizes from toluene.

The volatility of the lanthanide DMADB complexes increases as the radius of the metal ion decreases. Interestingly, even the polymeric lanthanide DMADB compounds are volatile and sublime readily without significant decomposition at temperatures below 100 °C.[32] The high volatility of the polymeric compounds suggests that there is a low barrier for depolymerization to form low molecular weight species (e.g., monomers and dimers). In contrast, and for reasons not well understood, attempts to sublime the isomorphous uranium analogues under identical conditions result only in thermal decomposition at elevated temperatures.[31]

Here, we present an analysis of the electronic structures of lanthanide and uranium DMADB complexes to identify the factors that may account for the differences in volatility. Density functional theory calculations, guided by field ionization mass spectrometry data, were used to identify the volatile lanthanide aminodiboranate species generated during sublimation, and to assess their relative stabilities.

■ COMPUTATIONAL AND EXPERIMENTAL DETAILS

DFT calculations were performed at the PBE[35]/def-TZVP[36−38] level using the *Turbomole 5.10.2* program.[39] Scalar relativistic effects were incorporated by employing effective core potentials (def-ECP) with 60 (U) and 28 (Er, Pr, Sm) core electrons, respectively;[36] spin−orbit effects were not included. The resolution of the identity approximation was introduced for the Coulomb integrals.[40,41] In addition, single point calculations were performed using the *Gaussian09* package.[42] As in the optimization, the PBE functional was employed. The Stuttgart/Dresden (SDD) basis set with the ECP60MWB_SEG core potential was used for U, whereas the SDD/ECP28MWB_SEG basis set was used for Sm, Pr, and Er.[37,43] The 6-311G(d,p) basis set was used on all nonmetal centers.[44] Integral evaluation was performed with an ultrafine grid and the nature of all stationary points was verified by vibrational analysis, which was subsequently used to compute the zero-point vibrational energies and molecular partition functions required to obtain thermal corrections to the energy. Mayer bond orders (MBOs)[45,46] were computed using the MN-GSM package together with a locally modified version of *Gaussian09*.[47] MBO analysis has been widely used to study lanthanide−ligand and actinide−ligand interactions.[48−50] The effect of long-range weak interactions (i.e., dispersion) between the large number of methyl groups present in the systems was included a posteriori using the DFT-D3 package developed by Grimme.[51,52] Standard PBE parameters with Becke and Johnson damping functions were used.[53−55] DFT, along with the use of ECP basis sets, has been used successfully for actinide and lanthanide containing systems.[55−63]

The $Ln(DMADB)_3$ complexes,[32,33] where Ln = Pr, Sm, and Er, and the two isomers of $U(DMADB)_3$,[30,31] were prepared as described previously. Field ionization mass spectra (FI-MS) were recorded on a Micromass 70-VSE mass spectrometer. The shapes of all peak envelopes correspond with those calculated from the natural abundance isotopic distributions in the observed spectra.

■ RESULTS AND DISCUSSION

Electronic Structure of Solid-State Uranium and Lanthanide Aminodiboranates Models. Understanding the factors that affect volatility is important for the development of practical CVD/ALD precursors. We have previously noted that *N*,*N*-dimethylaminodiboranate (DMADB) complexes of stoichiometry $M(DMADB)_3$ are highly volatile if the metal is a lanthanide but decompose under the same conditions without subliming if the metal is uranium.[30−33]

To determine the reasons for the difference in behavior, we performed density functional theory studies on finite size complexes. An oligomer model containing four metal centers (part a of Figure 3) gave metal−hydrogen distances that agreed well with those observed experimentally. The Er dimer was studied without truncation. For all of the $M^{III}(DMADB)_3$ species, the computed ground state is high spin as expected;

dx.doi.org/10.1021/jp305691y | J. Phys. Chem. C 2012, 116, 23194−23200

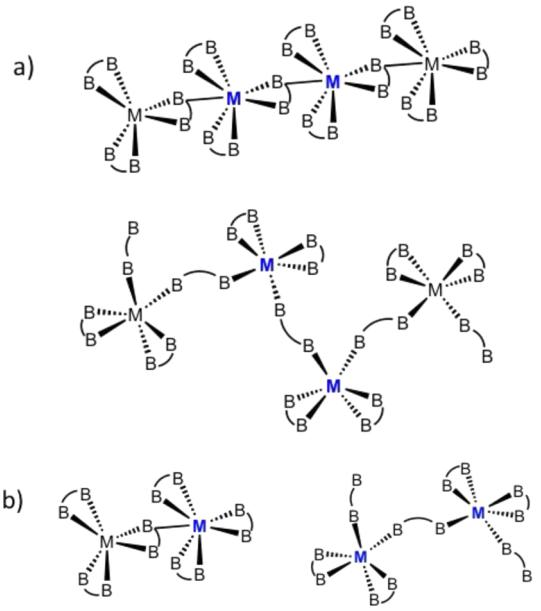

Figure 3. (a) Schematic representation of the tetrameric oligomers used to model the solid state polymeric chains. Metal centers whose distances are included in Table 1 are in blue. Top: $Sm_4(DMADB)_{12}$ and $U_4(DMADB)_{12}$ (U_A). Bottom: $[Pr_4(DMADB)_{13}]^-$ and $[U_4(DMADB)_{13}]^-$ (U_B). (b) Dimeric models used to compute Mayer bond orders. Left: $Sm_2(DMADB)_6$ and $U_2(DMADB)_6$ (U_A). Right: $[Pr_2(DMADB)_7]^-$ and $[U_2(DMADB)_7]^-$ (U_B). Metal centers whose bond orders are included in Table 1 are in blue.

thus, each trivalent metal center has two, five, three, and three unpaired electrons for Pr, Sm, Er, and U, respectively.

The optimized geometries are compared with available single crystal X-ray diffraction data in Table 1. Distances are reported for the two central metals in the truncated chains. The experimental positions of the hydrogen atoms can be determined less accurately than those of the boron atoms; however, theory gives good agreement with both experimental M−B and M−H distances. The computed and experimental B−N−B angles are very similar for the bridging ligands but can deviate up to two degrees for the chelating ligands (details in the Supporting Information). This deviation is also observed for the Er dimer, for which a truncated model was unnecessary, and thus is not an artifact of the model choice. The results suggest that the tetrameric oligomer is a good model of the infinite chain, and any small deviations in the metrical parameters are likely due to packing effects.

The molecular orbital picture is the same for all four metal complexes. The highest occupied orbitals are all singly occupied (SOMOs), and consist largely of localized 4f (or 5f) atomic orbitals that do not engage in bonding. Below the SOMOs are doubly occupied orbitals corresponding to delocalized bonding in the $-BH_3$ groups of the DMADB ligands (Supporting Information). These orbitals have little metal contribution and are qualitatively the same for the lanthanide and uranium species. All in all, the simple molecular orbital picture provides little if any information about why the actinide and lanthanide DMADB complexes behave differently when heated.

Mayer bond order analyses were performed on dimeric models of the metal DMADB complexes (part b of Figure 3 for Pr, Sm, and U, and part a of Figure 2 for Er) to quantify the nature of the M−H and M−B interactions (Table 1). Each individual bond has a small bond order of ∼0.35 for M−B and ∼0.2 for M−H. These values are only slightly smaller than those computed using a similar methodology for a high-spin iron borohydride compound.[61] Whereas it may seem surprising that the M−B bond order is larger than the M−H bond order, the molecular orbitals show that the electron density is distributed over the entire BH_3 group; therefore, it is likely that this electron density is contributing to the M−B bond order observed. Each M−B bond should be regarded as part of the interaction of the metal center with the entire BH_3 group rather than as a simple covalent M−B bond. For all of the compounds studied, the bond orders tend to increase as the metal ion becomes smaller. Interestingly, the bond orders are generally larger for the chelating ligands than for the bridging ligands suggesting that the M−H bonds to the bridging ligands are more likely to break when the compounds are heated. Furthermore, the difference in bond strengths between the U and isostructural Ln analogues is evident. In particular, the total M−H bond order for U_B is 0.62 larger than for the isostructural Pr species, and the total M−H bond order for U_A is 0.78 larger than for the isostructural Sm species. This result suggests that more energy will be required to depolymerize the uranium complexes than the lanthanide analogues.

Table 1. Selected Geometric Parameters Obtained from Ground State Geometry Optimization; Average Distances Are Reported for the Two Central Metal Centers (Part a of Figure 3) in Å; Average Individual Mayer Bond Orders Are Given along with the Number of Such Bonds Per Metal Center[a]

		Chelating DMADB Ligands				Bridging DMADB Ligands				Total Mayer Bond Order	
M		M−B dist	M−B MBO	M−H dist	M−H MBO	M−B dist	M−B MBO	M−H dist	M−H MBO	M−B	M−H
Pr	calcd	2.867	0.35 × 4	2.447	0.14 × 8	2.629	0.31 × 2	2.472	0.09 × 6	2.01	1.66
	exptl	2.877		2.443		2.666		2.469			
U_B	calcd	2.843	0.39 × 4	2.419	0.21 × 8	2.605	0.28 × 2	2.451	0.10 × 6	2.12	2.28
	exptl	2.879		2.487		2.667		2.498			
Sm	calcd	2.808	0.36 × 6	2.404	0.18 × 12	3.728	[b]	2.592	0.10 × 1	2.16[b]	2.26
	exptl	2.823		2.438		3.552		2.504			
U_A	calcd	2.815	0.41 × 6	2.398	0.24 × 12	3.623	[b]	2.486	0.16 × 1	2.46[b]	3.04
	exptl	2.885		2.494		3.524		2.495			
Er	calcd	2.723	0.36 × 4	2.335	0.22 × 8	2.684	0.44 × 2	2.324	0.20 × 4	2.32	2.56
	exptl	2.756		2.366		2.735		2.303			

[a]MBOs for dimers. Geometric parameters for the dimers are given in the Supporting Information. [b]No bond order computed for the bridging M−B interaction because a H atom is located in the bond path.

dx.doi.org/10.1021/jp305691y | J. Phys. Chem. C 2012, 116, 23194−23200

Fragmentation of the Solid-State Structures. During sublimation, the solid polymeric $M(DMADB)_3$ complexes must depolymerize by breaking metal−ligand bonds to generate volatile gas-phase species. To gain insights into the energetics of these bond breaking processes, we have carried out calculations of the energy required to remove a DMADB ligand from negatively charged $M(DMADB)_4^-$ species to form the neutral monomer. A schematic representation of the species examined in this study is given in Figure 4.

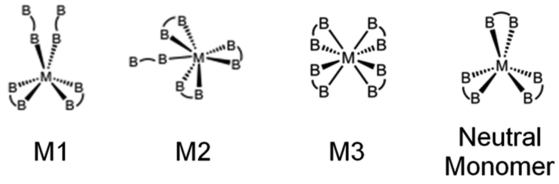

Figure 4. Schematic representation of the monomeric anions studied for M = U, Pr, Sm, and Er.

These structures were fully optimized. In all cases, the neutral monomer is 12-coordinate. For Pr and U, structure M1 has the same 14-coordinate geometry as seen in the solid state for these compounds. For Er, structure M1 optimizes to a 13-coordinate geometry instead of the 12-coordinate geometry seen in the solid state; one of the terminal ligands is bound by means of three hydrogen bridges instead of two. For Sm and U, M2 has a 14-coordinate environment in which the ligand that coordinates through only one B−H−M interaction in the solid state coordinates through two interactions. Finally, structure M3, which possesses four chelating ligands, allowed us to explore whether such structures with higher coordination numbers are energetically accessible. The coordination number decreases with the size of the ion: U is 15-coordinate, Pr and Sm are 14-coordinate, and Er is 12-coordinate.

The ligand dissociation energies for M1, M2, and M3 are presented in Table 2 as a function of the metal ion. Dispersion effects were particularly important, and were typically on the order of 5 kcal·mol^{-1}. (Note: unless otherwise specified all energies reported in the following text are dispersion-corrected free energies, ΔG_D. Table 2 gives both uncorrected ΔG and corrected ΔG_D values.) In most cases, more energy is required to remove a ligand from M3 than from M1 or M2. The data show that the smallest ligand dissociation energy (5.7 kcal·mol^{-1}) is seen for $Er(DMADB)_4^-$ versus 12.0 kcal·mol^{-1} for $Sm(DMADB)_4^-$ and 17.0 kcal·mol^{-1} for $Pr(DMADB)_4^-$. Thus, it becomes easier to form a neutral $M(DMADB)_3$ monomer by dissociation of a ligand as the lanthanide atom becomes smaller.

Table 2. Gibbs Free Energies and Dispersion Corrected Values in kcal·mol^{-1} for Removing a Ligand from M1, M2, and M3 Monomers

	Pr		Sm		Er		U	
	ΔG	ΔG_D	ΔG	ΔG_D	ΔG	ΔG_D	ΔG	ΔG_D
M1	12.9	17.0	[a]	[a]	1.3	5.7	14.6	19.1
M2	[a]	[a]	6.8	12.0	[a]	[a]	11.8	19.1
M3	11.4	19.3	9.6	17.3	0.2	9.7	14.6	20.2

[a]Not computed because this structure is not related to the experimental structure.

Despite the fact that Er^{3+} is the smallest lanthanide ion studied here and consequently the positive charge density at the metal center in $Er(DMADB)_3$ should be higher than that in its Pr and Sm analogues, our results show that the higher positive charge density does not lead to stronger metal−ligand binding as one would expect from a classical ionic bond model. Instead, saturating the metal coordination sphere and ligand relaxation play a key role in accounting for the observed trends. The dissociation energies reflect the energetic cost of removing a DMADB ligand from the M^{3+} coordination sphere and the energy required for the resulting under-coordinated complexes to rearrange to more favorable molecular geometries.

If we assume that these ligand dissociation energies for the $M(DMADB)_4^-$ species are correlated with the ligand dissociation energies required to depolymerize the solid state structures, then we would expect the volatility to increase in the order Pr < Sm < Er, as is in fact observed experimentally. All these trends are also correlated with the size of the lanthanide ion. The DMADB complex of the largest lanthanide in this series (Pr), which is a 14-coordinate polymer, is the least volatile, whereas the DMADB complex of the smallest lanthanide in this series (Er), which is a 12-coordinate dimer, is the most volatile.

Finally, the ligand dissociation energy of 19.1 kcal·mol^{-1} for the M1 and M2 structures of the U species $U(DMADB)_4^-$ is larger than those of all of the lanthanide $Ln(DMADB)_4^-$ compounds studied. Specifically, this energy is 7.1 kcal·mol^{-1} larger than its isostructural Sm analogue and 2.1 kcal·mol^{-1} larger than its isostructural Pr analogue. We point out that the Pr species is already the least volatile of the lanthanide compounds, and thus the U compound should require even more energy to convert its polymer into a monomeric form. This result is consistent with the experimental finding that the U complex decomposes under conditions at which the lanthanide complexes sublime.

Gas-Phase Species Present during CVD/ALD. The nature of the gas-phase species formed upon sublimation of the $M(DMADB)_3$ complexes has previously been investigated experimentally by positive-ion field ionization mass spectroscopy (FI-MS).[30,31] For the larger lanthanides Pr and Sm, mononuclear, dinuclear, and trinuclear species are detected in the FI-MS spectra; in most cases, one DMADB ligand has been lost to form these cationic species. In contrast, for Er, only mononuclear and dinuclear species are observed (Table 3).

Table 3. FI-MS Results for $Ln(DMADB)_3$[a]

	ML_2^+		ML_3^+		$M_2L_5^+$		$M_3L_8^+$	
M	mass	int.	mass	int.	mass	int.	mass	int.
Pr	285	35	356	65	642	35	999	10
Sm	296	95	367	80	660	100	1029	10
Er			381	100	693	15		

[a]Mass is given in m/z and the relative intensity in %.[32]

These results provide insight into the species actually present in the gas phase under CVD and ALD conditions, with the caveat that only neutral species are likely to be present under the latter conditions. Hence, the FI-MS results were used as a starting point for constructing the gas-phase models we analyzed computationally. Specifically, we investigated the mononuclear species $Ln(DMADB)_3$, the dinuclear species $Ln_2(DMADB)_6$, and the trinuclear species $Ln_3(DMADB)_9$.

dx.doi.org/10.1021/jp305691y | J. Phys. Chem. C 2012, 116, 23194−23200

Schematic representations of the structures considered are given in Figure 5 (the structure of the neutral monomer is given in Figure 4). No gas-phase structures of $U(DMADB)_3$ or its oligomers were investigated because this compound is not volatile.

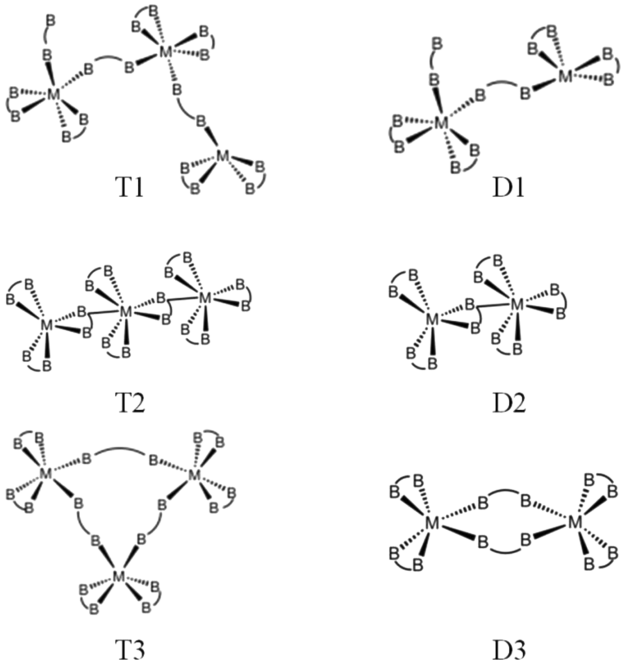

Figure 5. Gas-phase clusters studied for M = Pr, Sm, and Er. The DMADB ligand has been depicted schematically for simplicity. All of the structures shown are electrically neutral.

For $Pr(DMADB)_3$, the polymeric structure of the solid precursor can be cut to form the trimer denoted T1, in which one of the metal centers is only 11-coordinate. It is likely that this linear fragment will rearrange in such a way that all of the metal centers are 12-, 13-, or 14-coordinate; one possible rearranged structure is the cyclic structure T3. In fact, we calculate that this transformation is downhill energetically by $\Delta G_D = -9.3$ kcal·mol^{-1} (Table 4). Another possible structure is the acyclic trimer T2, and indeed our calculations show that the T1 to T2 rearrangement is downhill energetically by about the same amount, $\Delta G_D = -11.7$ kcal·mol^{-1}. Our results demonstrate that T1 is not present in the gas phase due to its instability with respect to both T2 and T3. For $Sm(DMADB)_3$, structure T2 is closely related to the experimental solid-state structure. Our calculations show that it is 7.0 kcal·mol^{-1} more stable than structure T3.

Table 4. Gibbs Free Energies of Isomerization Reactions in the Gas Phase (And Dispersion Corrected Values) Reported in kcal·mol^{-1}

Pr	ΔG	ΔG_D
T1 → T2	−18.3	−11.7
T1 → T3	−19.8	−9.3
T2 → T3	−1.5	2.4
D1 → D2	−16.2	−21.3
D1 → D3	−21.4	−25.4
D2 → D3	−5.2	−4.1
Sm	ΔG	ΔG_D
T2 → T3	4.0	7.0
D2 → D3	2.1	3.4

Turning to dinuclear species, we first note that structure D1 is again a fragment of the polymeric structure seen for $Pr(DMADB)_3$. As before, one of the metal centers is only 11-coordinate, and rearrangement should occur to form structures such as D2 or D3. In fact, we calculate that structure D1 is highly unstable with respect to both D2 and D3, and that conversion to the latter is downhill energetically by $\Delta G_D = -21.3$ and -25.4 kcal·mol^{-1}, respectively. For $Sm(DMADB)_3$, structure D2 most closely resembles the solid-state structure. Once again, our calculations show that D2 is 3.4 kcal·mol^{-1} more stable than structure D3.

Furthermore, our DFT results demonstrate that the lowest energy trimers are unstable with respect to decomposition into the dimer and the neutral monomer, as shown in Table 5. FI-MS data support this conclusion because the relative intensities are much lower for the trimers than for the dimers and monomers. Dispersion effects play an important role in the stability of the dimeric species with respect to the monomeric species for both Sm and Pr. When dispersion is accounted for, the dimers are more stable than the monomers, although only by a few kcal·mol^{-1}. In contrast, for Er the calculations show that the monomers are more stable than the dimers by 7.6 kcal·mol^{-1}.

Table 5. Gibbs Free Energies (And Dispersion Corrected Values) in kcal·mol^{-1} for the Decomposition of Gas-Phase Clusters (M = the Neutral Monomer $Ln(DMADB)_3$)

		ΔG	ΔG_D
Pr	T3 → D3 + M	−13.3	−5.4
	T2 → D3 + M	−14.8	−3.0
	D3 → 2M	−5.0	2.7
Sm	T2 → D2 + M	−14.2	−5.7
	D2 → 2M	−7.6	1.4
Er	D3 → 2M	−16.5	−7.6

Thus, we conclude that the Er precursor, which is a dimer in the solid state, probably sublimes as a monomer. This finding is supported by the relative intensities of the peaks in the FI-MS spectra: the ErL_3^+ peak has a relative intensity of 100%, whereas the $Er_2L_5^+$ peak has a relative intensity of only 15%.

The relative stabilities of the monomers and dimers are again consistent with expectations based on ionic radii. Monomers are relatively more stable for smaller lanthanides such as Er, whereas dimers are relatively more stable for larger lanthanides such as Sm and Pr. For all three lanthanides, the monomer has a coordination number of 12, which is equal to the experimental coordination number seen in the crystal structures for Er but less than the coordination numbers of 13 and 14 seen for the Sm and Pr complexes. For the larger lanthanides, the dimeric structures are favored because they permit the ligands to form more Ln−H bonds with the metal centers.

CONCLUSIONS

The observed decrease in the volatility of $Ln(DMADB)_3$ complexes with an increase in the size of the lanthanide ion is a result of the larger energy required to break the metal−DMADB bonds, a process that is necessary to convert the solid state species (which are oligomers or polymers with bridging DMADB ligands). Neutral gas-phase species from monomers to trimers were studied and long-range weak interactions

dx.doi.org/10.1021/jp305691y | J. Phys. Chem. C 2012, 116, 23194−23200

(dispersion) were found to make significant contributions to the energies of these species. The Sm oligomers in the gas phase maintain the connectivity of the solid state, whereas the Pr species undergo ligand rearrangement. In all cases, trimeric and dimeric structures are unstable and readily decompose into monomers in the gas phase, and the relative energies of these species are correlated with their relative intensities as determined by FI-MS. For Sm and Pr, the monomers and dimers have similar stabilities and exist in equilibrium in the gas phase. In contrast, the Er dimer is unstable in the gas phase with respect to the neutral monomer. Mayer bond orders demonstrated that the M−H bonds are stronger for the uranium species than their lanthanide analogues, which explains why $U(DMADB)_3$ decomposes rather than sublimes when it is heated.

■ ASSOCIATED CONTENT

Supporting Information

Coordinates and additional discussion is provided. This material is available free of charge via the Internet at http://pubs.acs.org.

■ AUTHOR INFORMATION

Corresponding Author

*E-mail: gagliard@umn.edu (L.G.), girolami@scs.uiuc.edu (G.G.).

Present Address

‡Department of Chemistry, The George Washington University, 725 21st Street, NW, Washington, DC 20052.

Author Contributions

All authors have given approval to the final version of the manuscript.

Notes

The authors declare no competing financial interest.

■ ACKNOWLEDGMENTS

The authors would like to acknowledge Danylo Zherebetskyy for useful discussions. This research was supported by Director, Office of Basic Energy Sciences, U.S. Department of Energy under Contract No. USDOE/DESC002183. We also acknowledge support from the U.S. National Science Foundation under grant CHE-0952054 for support for PM and CJC and under grant CHE 11-12360 to GSG. Finally, we thank the PG Research Foundation for support of S.R.D.

■ REFERENCES

(1) Bunzli, J. C. G.; Piguet, C. *Chem. Soc. Rev.* **2005**, *34* (12), 1048−1077.

(2) Kido, J.; Okamoto, Y. *Chem. Rev.* **2002**, *102* (6), 2357−2368.

(3) Carlos, L. D.; Ferreira, R. A. S.; Bermudez, V. D.; Ribeiro, S. J. L. *Adv. Mater.* **2009**, *21* (5), 509−534.

(4) Etourneau, J. *J. Less-Common Met.* **1985**, *110* (1−2), 267−281.

(5) Gasgnier, M. *J. Mater. Sci.* **1991**, *26* (8), 1989−1999.

(6) Collocott, S. J.; Dunlop, J. B.; Lovatt, H. C.; Ramsden, V. S. *Mater. Sci. Forum* **1999**, *315−317*, 77−83.

(7) Robertson, J. *Eur. Phys. J.:Appl. Phys.* **2004**, *28* (3), 265−291.

(8) Scullin, M. L.; Yu, C.; Huijben, M.; Mukerjee, S.; Seidel, J.; Zhan, Q.; Moore, J.; Majumdar, A.; Ramesh, R. *Appl. Phys. Lett.* **2008**, *92* (20), 202113.

(9) Crowell, J. E. *J. Vac. Sci. Technol. A* **2003**, *21* (5), S88−S95.

(10) Yanguas-Gil, A.; Yang, Y.; Kumar, N.; Abelson, J. R. *J. Vac. Sci. Technol. A* **2009**, *27* (5), 1235−1243.

(11) George, S. M. *Chem. Rev.* **2010**, *110* (1), 111−131.

(12) Jensen, J. A.; Gozum, J. E.; Pollina, D. M.; Girolami, G. S. *J. Am. Chem. Soc.* **1988**, *110* (5), 1643−1644.

(13) Kumar, N.; Yang, Y.; Noh, W.; Girolami, G. S.; Abelson, J. R. *Chem. Mater.* **2007**, *19* (15), 3802−3807.

(14) Kumar, N.; Yanguas-Gil, A.; Daly, S. R.; Girolami, G. S.; Abelson, J. R. *J. Am. Chem. Soc.* **2008**, *130* (52), 17660−17661.

(15) Sung, J. W.; Goedde, D. M.; Girolami, G. S.; Abelson, J. R. *J. Appl. Phys.* **2002**, *91* (6), 3904−3911.

(16) Jayaraman, S.; Yang, Y.; Kim, D. Y.; Girolami, G. S.; Abelson, J. R. *J. Vac. Sci. Technol. A* **2005**, *23* (6), 1619−1625.

(17) Jayaraman, S.; Gerbi, J. E.; Yang, Y.; Kim, D. Y.; Chatterjee, A.; Bellon, P.; Girolami, G. S.; Chevalier, J. P.; Abelson, J. R. *Surf. Coat. Technol.* **2006**, *200* (22−23), 6629−6633.

(18) Yang, Y.; Jayaraman, S.; Kim, D. Y.; Girolami, G. S.; Abelson, J. R. *Chem. Mater.* **2006**, *18* (21), 5088−5096.

(19) Yang, Y.; Jayaraman, S.; Kim, D. Y.; Girolami, G. S.; Abelson, J. R. *J. Cryst. Growth* **2006**, *294* (2), 389−395.

(20) Yang, Y.; Jayaraman, S.; Sperling, B.; Kim, D. Y.; Girolami, G. S.; Abelson, J. R. *J. Vac. Sci. Technol. A* **2007**, *25* (1), 200−206.

(21) Zange, E. *Chem. Ber.* **1960**, *93* (3), 652−657.

(22) Mirsaidov, U.; Shaimuradov, I. B.; Khikmatov, M. *Russ. J. Inorg. Chem.* **1986**, *31* (5), 1321−1323.

(23) Shaimuradov, I. B.; Badalov, A. B.; Marufi, V. K.; Mirsaidov, U. *Russ. J. Inorg. Chem.* **1991**, *36* (5), 1353−1353.

(24) Shinomoto, R.; Zalkin, A.; Edelstein, N. M. *Inorg. Chim. Acta* **1987**, *139* (1−2), 97−101.

(25) White, J. P.; Deng, H. B.; Shore, S. G. *Inorg. Chem.* **1991**, *30* (10), 2337−2342.

(26) Schlesinger, H. I.; Brown, H. C. *J. Am. Chem. Soc.* **1953**, *75* (1), 219−221.

(27) Bernstein, E. R.; Hamilton, W. C.; Keiderling, T. A.; La Placa, S. J.; Lippard, S. J.; Mayerle, J. J. *Inorg. Chem.* **1972**, *11* (12), 3009−3016.

(28) Shinomoto, R.; Gamp, E.; Edelstein, N. M.; Templeton, D. H.; Zalkin, A. *Inorg. Chem.* **1983**, *22* (17), 2351−2355.

(29) Ephritikhine, M. *Chem. Rev.* **1997**, *97* (6), 2193−2242.

(30) Daly, S. R.; Girolami, G. S. *Chem. Commun.* **2010**, *46* (3), 407−408.

(31) Daly, S. R.; Girolami, G. S. *Inorg. Chem.* **2010**, *49* (11), 5157−5166.

(32) Daly, S. R.; Kim, D. Y.; Yang, Y.; Abelson, J. R.; Girolami, G. S. *J. Am. Chem. Soc.* **2010**, *132* (7), 2106−2107.

(33) Daly, S. R.; Kim, D. Y.; Girolami, G. S. *Inorg. Chem.* **2012**, *51*, 7050−7065.

(34) Shannon, R. D. *Acta Crystallogr., Sect. A* **1976**, *32* (Sep1), 751−767.

(35) Perdew, J. P.; Burke, K.; Ernzerhof, M. *Phys. Rev. Lett.* **1997**, *78* (7), 1396−1396.

(36) Cao, X. Y.; Dolg, M. *J. Chem. Phys.* **2001**, *115* (16), 7348−7355.

(37) Cao, X. Y.; Dolg, M. *J. Mol. Struc.-Theochem* **2002**, *581*, 139−147.

(38) Cao, X. Y.; Dolg, M. *J. Mol. Struc.-Theochem* **2004**, *673* (1−3), 203−209.

(39) Ahlrichs, R.; Bar, M.; Haser, M.; Horn, H.; Kolmel, C. *Chem. Phys. Lett.* **1989**, *162* (3), 165−169.

(40) Eichkorn, K.; Treutler, O.; Ohm, H.; Haser, M.; Ahlrichs, R. *Chem. Phys. Lett.* **1995**, *242* (6), 652−660.

(41) Eichkorn, K.; Weigend, F.; Treutler, O.; Ahlrichs, R. *Theor. Chem. Acc.* **1997**, *97* (1−4), 119−124.

(42) Frisch, M. J.; Trucks, G. W.; Schlegel, H. B.; Scuseria, G. E.; Robb, M. A.; Cheeseman, J. R.; Scalmani, G.; Barone, V.; Mennucci, B.; Petersson, G. A., et al. *Gaussian 09*, Rev. A.1; Gaussian, Inc.: Wallingford, 2009.

(43) Dolg, M.; Stoll, H.; Preuss, H. *J. Chem. Phys.* **1989**, *90* (3), 1730−1734.

(44) Krishnan, R.; Binkley, J. S.; Seeger, R.; Pople, J. A. *J. Chem. Phys.* **1980**, *72* (1), 650−654.

(45) Mayer, I. *Chem. Phys. Lett.* **1983**, *97* (3), 270−274.

(46) Bridgeman, A. J.; Cavigliasso, G.; Ireland, L. R.; Rothery, J. *J. Chem. Soc., Dalton Trans.* **2001**, No. 14, 2095−2108.

(47) Olson, R. M.; Marenich, A. V.; Chamberlin, A. C.; Kelly, C. P.; Thompson, J. D.; Xidos, J. D.; Li, J.; Hawkins, G. D.; Winget, P. D.; Zhu, T.; Rinaldi, D., et al. MN-GSM version 2011, University of Minnesota, Minneapolis, MN 55455−0431, 2011.
(48) Lyon, J. T.; Hu, H. S.; Andrews, L.; Li, J. *Proc. Nat. Acad. Sci. U.S.A.* **2007**, *104* (48), 18919−18924.
(49) Arnold, P. L.; Turner, Z. R.; Kaltsoyannis, N.; Pelekanaki, P.; Bellabarba, R. M.; Tooze, R. P. *Chem.—Eur. J.* **2010**, *16* (31), 9623−9629.
(50) Xu, W. H.; Jin, X.; Chen, M. H.; Pyykko, P.; Zhou, M. F.; Li, J. *Chem. Sci.* **2012**, *3* (5), 1548−1554.
(51) Grimme, S.; Antony, J.; Ehrlich, S.; Krieg, H. *J. Chem. Phys.* **2010**, *132* (15), 154104.
(52) Grimme, S.; Ehrlich, S.; Goerigk, L. *J. Comput. Chem.* **2011**, *32* (7), 1456−1465.
(53) Becke, A. D.; Johnson, E. R. *J. Chem. Phys.* **2005**, *122*, 154101.
(54) Johnson, E. R.; Becke, A. D. *J. Chem. Phys.* **2005**, *123*, 024101.
(55) Johnson, E. R.; Becke, A. D. *J. Chem. Phys.* **2006**, *124*, 174104.
(56) Schreckenbach, G.; Shamov, G. A. *Acc. Chem. Res.* **2010**, *43* (1), 19−29.
(57) Schreckenbach, G.; Hay, P. J.; Martin, R. L. *J. Comput. Chem.* **1999**, *20* (1), 70−90.
(58) Cundari, T. R.; Stevens, W. J. *J. Chem. Phys.* **1993**, *98* (7), 5555−5565.
(59) Cundari, T. R.; Sommerer, S. O.; Strohecker, L. A.; Tippett, L. *J. Chem. Phys.* **1995**, *103* (16), 7058−7063.
(60) Jeletic, M.; Lin, P. H.; Le Roy, J. J.; Korobkov, I.; Gorelsky, S. I.; Murugesu, M. *J. Am. Chem. Soc.* **2011**, *133* (48), 19286−19289.
(61) Mehn, M. P.; Brown, S. D.; Paine, T. K.; Brennessel, W. W.; Cramer, C. J.; Peters, J. C.; Que, L. *Dalton Trans.* **2006**, No. 10, 1347−1351.
(62) MacDonald, M. R.; Bates, J. E.; Fieser, M. E.; Ziller, J. W.; Furche, F.; Evans, W. J. *J. Am. Chem. Soc.* **2012**, *134* (20), 8420−8423.
(63) Siladke, N. A.; Meihaus, K. R.; Ziller, J. W.; Fang, M.; Furche, F.; Long, J. R.; Evans, W. J. *J. Am. Chem. Soc.* **2012**, *134* (2), 1243−1249.